Nanoparticle amount, and not size, determines chain alignment and nonlinear hardening in polymer nanocomposites

H. Samet Varol [a], Fanlong Meng [b], Babak Hosseinkhani [d], Christian Malm [a], Daniel Bonn [e], Mischa Bonn [a], Alessio Zaccone [b,c], Sapun H. Parekh [a]

[a] Department of Molecular Spectroscopy, Max Planck Institute for Polymer Research, Mainz, Germany

[b] Cavendish Laboratory, University of Cambridge, CB3 0HE Cambridge, U.K.

[c] Department of Chemical Engineering and Biotechnology, University of Cambridge, CB2 3RA Cambridge, U.K.

[d] SKF Engineering & Research Center, Nieuwegein, The Netherlands

[e] Institute of Physics, University of Amsterdam, Amsterdam, The Netherlands.

Classification: Physical Sciences (Applied Physical Sciences)

Keywords: nanocomposites, polymer bridging, nonlinear elasticity, strain-hardening, polymer chain alignment

Corresponding Author

Sapun H. Parekh

Address: Molecular Spectroscopy Department, Max Planck Institute for Polymer Research

Ackermannweg 10, 55128 Mainz (Germany)

E-mail address: parekh@mpip-mainz.mpg.de

Abstract

Polymer nanocomposites – a polymer matrix blended with nanoparticles – strengthen under sufficiently large strains. Such strain hardening is critical to their function, especially for materials that bear large cyclic loads such as car tires or bearing sealants. While the reinforcement (i.e. the increase in the *linear* elasticity) by the addition of filler particles is phenomenologically understood, considerably less is known about strain hardening (the *nonlinear* elasticity). Here, we elucidate the molecular origin of strain hardening using uniaxial tensile loading, micro-spectroscopy of polymer chain alignment, and theory. The strain-hardening modulus and chain alignment are found to depend on the volume fraction, but not the size of nanofillers. This contrasts with reinforcement, which depends on both volume fraction *and* size of nanofillers, allowing linear and nonlinear elasticity of nanocomposites to be tuned independently.

Significance Statement

When straining materials (e.g. pulling a rubber band), they initially deform in proportion to the strain; if one pulls harder, some materials strengthen. This phenomenon, known as nonlinear strain hardening, is a critical feature of composite polymer materials – polymers with reinforcing filler particles – used in e.g. car tires. Engineering properties such as modulus, toughness, and strength of nanocomposites have been traditionally optimized through trial-and-error by changing the size and amount of fillers. Our work elucidates the molecular origin of strain hardening in polymer nanocomposites, showing that filler amount, but not size, sets the strain-hardening properties based on inter-filler chain elongation. The insensitivity to filler size provides a facile concept to independently tune linear and nonlinear mechanics in composites.

\body

Introduction

Many synthetic and natural materials around us increase their elastic modulus upon large deformation; a phenomenon that is known as work or *strain hardening*, which is critical to their function. In ductile polymer materials, the strain-hardening behaviour is essential for their functional lifetime, resilience, and toughness – all key parameters of their practical uses – because these materials repetitively bear large loads.(1, 2) Many industrial and consumer polymeric materials are composites, in which (hard) nanoscale inorganic particles, or fillers, are blended with polymer matrices to tailor their mechanical properties. In preparing such nanocomposites, filler-filler and filler-matrix interaction, filler dispersion, and polymer properties all affect the linear (mechanical reinforcement) and nonlinear (strain softening and strain hardening) mechanical response in nontrivial ways.(3) While a massive volume of work has attempted to clarify the mechanism of reinforcement (increased linear elasticity) at low strain and of nonlinear strain softening (the Payne and Mullins effects) at medium strain, a comparatively much smaller body of work exists that focuses on the mechanism of strain hardening in polymer composite materials.

In analogy to rubber elasticity, strain hardening in polymer composites is typically attributed to the resistance to deformation of extended and oriented polymer chains. (4–7) However, it has been shown that polymer chain alignment during strain hardening is strongly affected by dispersing fillers within the host polymer matrix.(8–10) To account for these observations, one needs to establish the relation between the macroscopically observed strain hardening and the microscopic chain alignment that is affected by the presence of fillers.

The connection between chain alignment and strain hardening in glassy polymer composites is purported to occur because the fillers act as “entanglement attractors”. In this picture, the segmental mobility of the polymer is disturbed (e.g. strongly constrained) by the presence of a large amount of surface area of the nanofillers, causing an increase in the number of physical entanglements. This results in greater alignment of effectively shorter segments between entanglement points in response to the applied load.(8, 11) Consistent with this idea, Jancar *et al*. showed that encapsulating micron-sized fillers in poly (methyl methacrylate) (PMMA) had negligible effect on the strain-hardening properties of the PMMA matrix as opposed to the inclusion of the same volume fraction of

nanofillers, which induced substantial strain hardening.(8) This suggests a clear role for both filler size and amount on strain hardening. However, because of the high glass transition temperature (T_g) for PMMA, simultaneous measurement of chain alignment was not possible in these experiments. Measuring chain alignment as a function of deformation in real-time is possible in elastomer-based nanocomposites, which have a T_g well below room temperature. This allows investigation of the effect of nanofiller size and volume fraction on strain hardening and chain alignment simultaneously; previous studies have focused on either mechanical strain hardening(12–15) or chain alignment,(16–19) but not both.

We investigate the strain-hardening mechanics and chain alignment in cross-linked, uniaxially loaded acrylonitrile butadiene rubber (NBR) nanocomposites (T_g ~ -30 °C) containing different amounts and sizes of SiO_2 nanofillers. Filler aggregate dispersion in different composites was imaged using transmission electron microscopy (TEM). Strain hardening was quantified by the strain-hardening or neo-Hookean modulus (G_p), measured in uniaxial tensile tests.(20, 21) Combined with polarized Raman micro-spectroscopy measurements of chain alignment *during* uniaxial deformation, we find that G_p is directly proportional to chain alignment and both depend on filler volume fraction, but are surprisingly independent of filler size and morphology. Using a simple scaling argument, we show that the observed chain alignment is dominated by "bridging" chains between filler aggregates. We find that chain alignment is independent of filler size because of a coupling between inter-filler spacing (related to bridging chain alignment) and volume fraction of fillers (related to total amount of bridging chains that become aligned). This demonstrates a clear distinction between the origin of nonlinear strain hardening (for which we find the nanofiller size to be irrelevant) and linear reinforcement (for which nanofiller size is important)(22) for nanocomposite-materials.

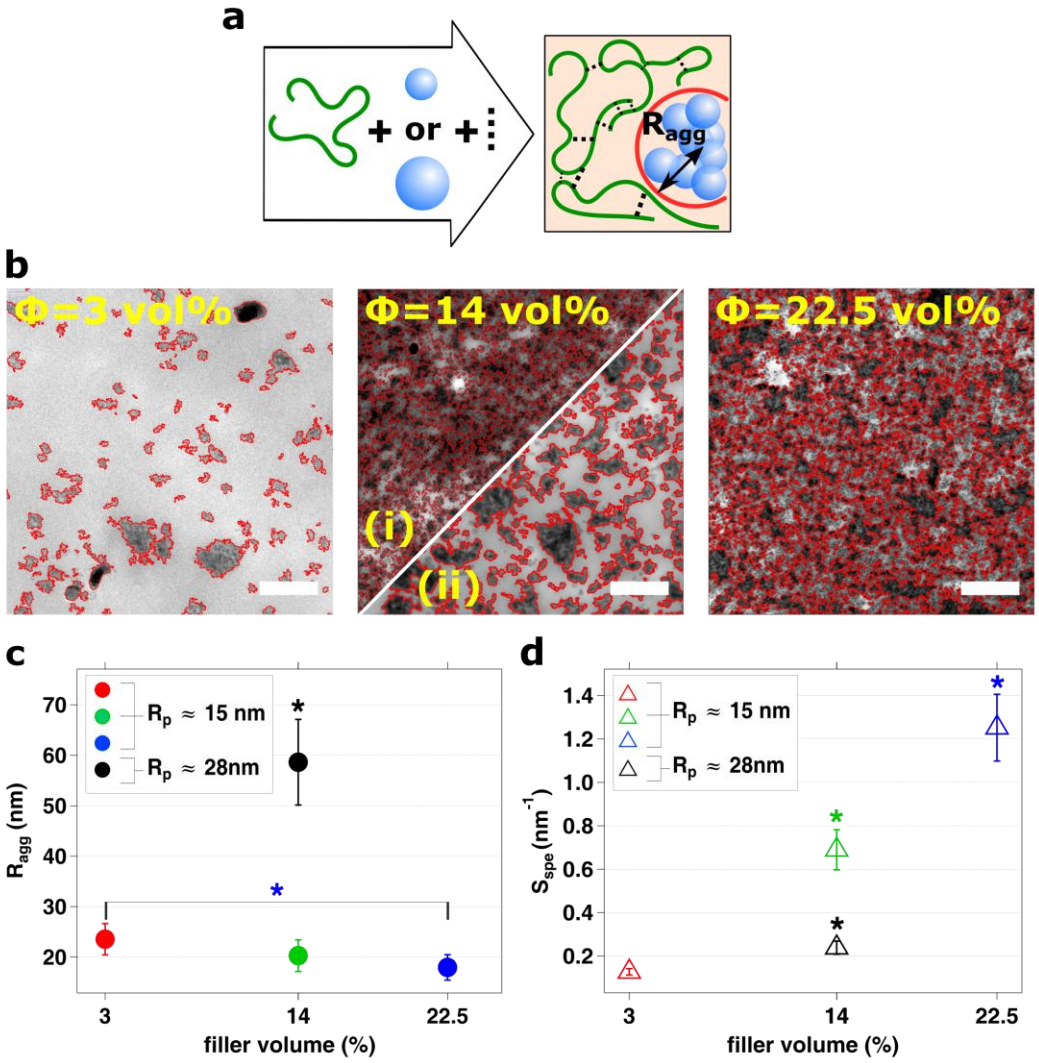

Figure 1. Formulation and ultrastructural characterization of nanocomposite materials. (a) Main ingredients and final microstructure of the SiO_2 / NBR nanocomposites are illustrated. Green curved line and black dashed line represents NBR molecule and sulfur cross-links, respectively. The two different sized blue balls represent the largest and smallest size nanofillers. (b) TEM images after image analysis of SiO_2 / NBR composites with different volume fraction (Φ) and primary particle size (R_p) of fillers. (i) and (ii) in the centre image both have Φ = 14%, with smallest (R_p = 15 nm) and largest (R_p = 28 nm) particles, respectively. Scale bars are 1µm. (c) Average aggregate sizes (R_{agg}) and (d) specific surface area (S_{spe}) of these samples computed by image analysis. Error bars are standard error of mean (s.e.m.) from at least 4000 aggregates from each nanocomposite. Asterisks present the significant differences ($p < 0.05$) of R_{agg} and S_{spe} (1-way ANOVA with Tukey's tests).

Nanocomposite morphology

It was shown previously that the linear viscoelastic properties (reinforcement) of elastomer composite materials scaled with both the amount *and* size of dispersed nano- and microfillers for numerous elastomer polymer composites.(22) Here, we focus on elastomer nanocomposites made from acrylonitrile butadiene rubber (NBR, M_w = 250000 g/mol) loaded with various amounts (quantified as the volume fraction, Φ) and sizes (R_p) of silica (SiO_2) nanofillers. The nanocomposites are produced by melt processing and mixing (see Methods). Figure 1a shows the basic formulation of the nanocomposites studied here, which contain NBR (green) and one of the two different primary particle sizes (R_p) fillers (blue). All nanocomposites are vulcanized (cross-linked) (Fig. 1a, black dotted lines). Importantly, no additional coating or coupling agents are used in these composites to modulate filler-NBR interaction so that the composite system is as simple as possible.

Figure 1b shows transmission electron microscope (TEM) images of ultracryotomed sections of the four different nanocomposite formulations studied in this work. Light and dark contrast regions in micrographs show the elastomeric matrix and silica aggregates, respectively. Image analysis of TEM micrographs was used to quantify the filler aggregate size (R_{agg}) and dispersion(23). Aggregate outlines are depicted by red borders in each micrograph shown in Figure 1b. From left to right, composites contain increasing Φ with Φ = 3%, 14%, and 22.5%, respectively. The two images with Φ = 14% contain different R_p (15 and 28 nm) whereas all other images contain R_p = 15 nm. Histograms of all detected aggregates from each nanocomposite are shown in Figure S1. Because a normal (Gaussian) distribution does not accurately fit these histograms, we used a weighted average over the histogram for those events that comprised 90% of the detected aggregate areas to calculate a mean aggregate size, R_{agg} (see Methods). This reduces the influence of aggregate outliers with very low abundance on R_{agg}.

Figure 1c show values for R_{agg} of each composite. With R_p = 15 nm, R_{agg} = 20 ± 3 nm (mean ± standard error of the mean) for Φ = 14% and 22.5% and R_{agg} increases slightly to 23.5 ± 3 nm for Φ = 3%. At Φ = 14% and R_p = 28 nm, R_{agg} = 59 ± 8.5 nm. A straightforward metric to evaluate Φ and R_{agg} simultaneously is the specific surface area (S_{spe}=Φ/R_{agg}) (Fig. 1d). Interestingly, samples with low concentrations of small particles (Φ = 3%, R_p = 15 nm) and higher concentrations of large particles (Φ = 14% R_p = 28 nm) resulted in composites with similar S_{spe}. Therefore, this sample set allows us to

independently investigate the impact of filler volume fraction and filler size on the strain-hardening behavior of real industrial nanomaterials.

Nanocomposite strain hardening under tensile loads

We quantified the effect of filler size and Φ on strain hardening of the nanocomposites using tensile tests. True stress (σ_{True}) – true strain (ε_{True}) curves of NBR composites, are shown in Figure 2a. Engineering stress (σ_{eng}) and strain (ε_{eng}) curves are shown as Figure S2 for reference. The curves in Figure 2a end abruptly because of composite fracture. All composites showed strain hardening at large strains (and showed no evidence of necking). Immediately obvious from Fig. 2a is the increased strain hardening at lower strain levels for increasing Φ. Interestingly, the curves with both sizes of fillers with Φ =14% appear indistinguishable. Moreover, the strain hardening curves for neat NBR and for the composite with Φ = 3% also closely overlay.

In order to quantify the strain hardening for the data presented in Figure 2a, we calculated the strain hardening modulus, G_p. This modulus, also known as the neo-Hookean modulus derived by Mooney,(24) was used by Hawards and Thackray(25) to model cross-linked polymer composite networks as a nonlinear (rubbery) spring in parallel with a Eyring dashpot (fillers), and another Hookean spring (fillers). (12, 13, 26–28) In this model, randomly cross-linked (vulcanized) NBR chains create a network made up of freely joined chains, which are entropic springs that stiffen under volume conserving extension leading to(5, 20):

$$\sigma_{True} = G_p\left(\lambda^2 - \frac{1}{\lambda}\right), \text{where } \lambda = \varepsilon_{Eng} + 1 \text{ and } G_p \text{ is the strain hardening modulus.}$$

This relation allows one to effectively quantify the linear and nonlinear behaviour simultaneously with G_p due to the scaling of $\left(\lambda^2 - \frac{1}{\lambda}\right)$ under the assumption of Gaussian chain statistics. Figure 2b shows Gaussian (or neo-Hookean) plots of each NBR systems until their fracture points. Since each of the composites fractured at different strain, we focus on the region from ε_{eng} = 0 - 2.9 (0 - 14.95 in the Gaussian plots) as this is the maximum strain all composites could sustain (Fig. 2b, red box). This region is shown highlighted in Fig. 2c. Comparing G_p from different samples for the different nanocomposites, we mark statistically significant differences (p < 0.05) between each pair of composites by grey boxes in the box chart (inset, Fig. 2c). Consistent with data in Fig. 2b, G_p is statistically identical for both samples with Φ = 14% and for neat NBR and Φ = 3%. Figure 2d further

shows the trend that G_p increases linearly with Φ, independent of filler size, for a variety of NBR nanocomposite formulations. Statistical testing of G_p in many different NBR samples confirmed the finding that G_p varied only with Φ and was independent of filler size (Fig. S4), which is contrary to reinforcement in the same samples.

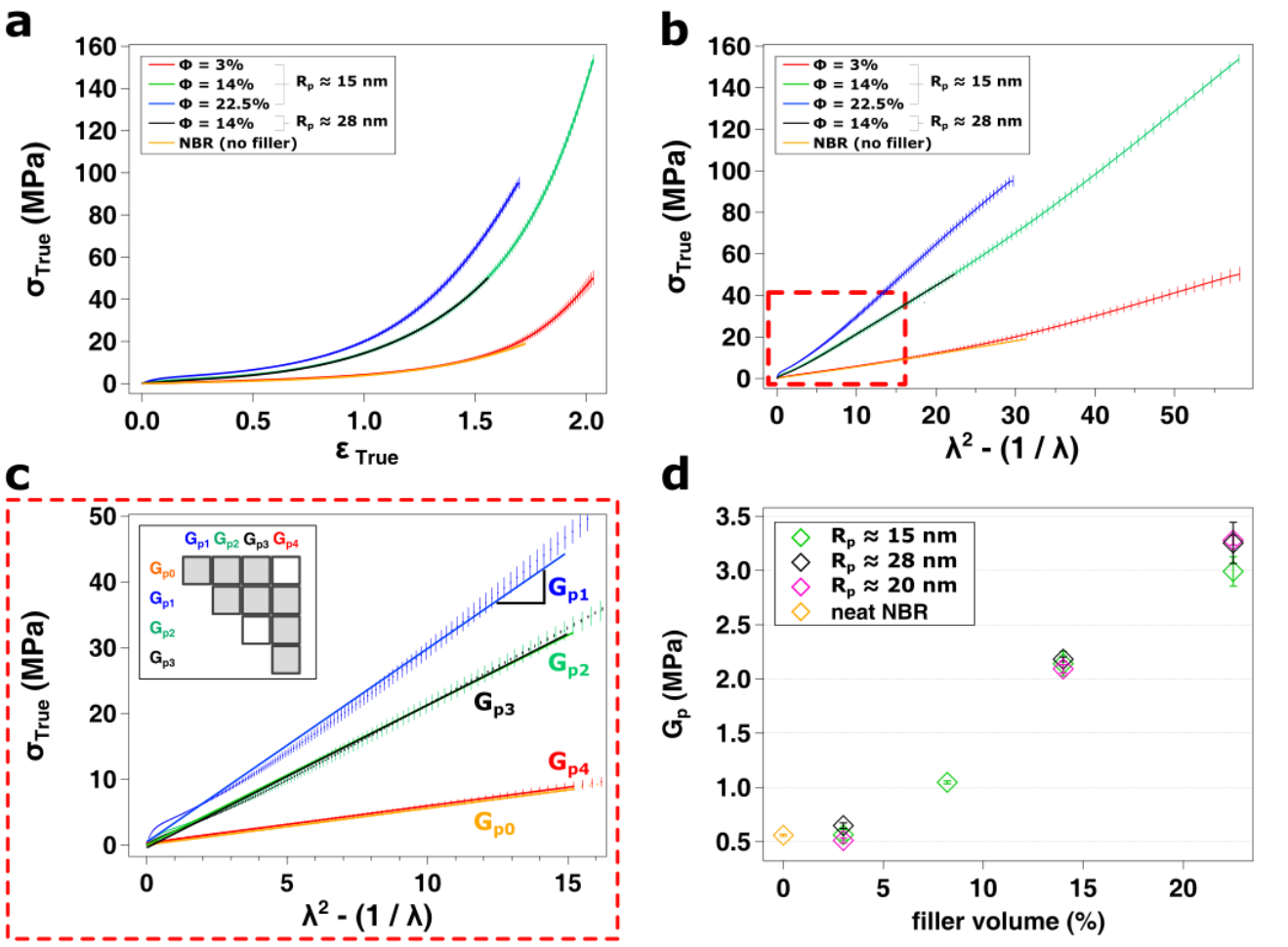

Figure 2. Strain-hardening characteristics of nanocomposites. (a) True stress (σ_{True}) – true strain (ε_{True}) curves of SiO_2 / NBR nanocomposites with different filler volume and size. σ_{True} - ε_{True} of the unfilled (vulcanized) NBR is shown by the orange curve. (b) Gaussian plots of σ_{True} as a function of (λ^2-1/ λ) of all the NBR systems. (c) Zoom into the red box shown in (b) presenting the G_p of each sample between the region where ε_{eng} is between 0 and 2.9. Inset is a box chart where statistically significant differences ($p < 0.05$) between G_p of each pair of composites is denoted by a grey box (2 tailed t-test). (d) G_p derived from Gaussian plots of many NBR nanocomposites containing different Φ and R_p of fillers. Error bars are standard deviation (s.d.) of three independent measurements of three slices from the same composite slab.

***In situ* chain alignment during nanocomposite uniaxial stretching**

We used *in situ* vibrational spectroscopy to measure molecular chain alignment during uniaxial tension application using polarized Raman micro-spectroscopy. In our measurements, the sample was rotated such that the Raman excitation laser was polarized parallel or perpendicular to the loading direction at each strain level (ε_{eng}), and all Raman scattered light was detected; there was no polarizer in front of the detector as we were uninterested in depolarization ratios. Raman spectra at each ε_{eng} were recorded as $A_{\parallel}$ or $A_{\perp}$, depending on whether the laser polarization was parallel or perpendicular to the stretching direction, respectively. We calculated the $\langle \boldsymbol{P_2} \rangle$ coefficient from these amplitudes and refer to this coefficient as the molecular order parameter, $S_{mol} = \frac{A_{\parallel} - A_{\perp}}{A_{\parallel} + 2\,A_{\perp}}$.(17, 29) S_{mol} is zero for a perfectly isotropic vibration. For a perfectly anisotropic vibrational mode of a molecular group aligned parallel or orthogonal to the loading direction S_{mol} is 1 or -0.5, respectively. In the case of stretching vibrations, such as the C≡N or C=C stretches, the polarizability changes as nuclei move along the bond axis, so S_{mol} reflects bond orientation.

An important challenge of polarized Raman measurements is spectral normalization to account for spatial heterogeneity from different positions and for inter-sample comparison. This is critical for obtaining an accurate measurement of S_{mol} and comparing measurements within and among nanocomposites. We verified that it was possible to use vibrational modes that exhibit no anisotropy as normalizing vibrations with measurements in amorphous polystyrene as a reference. Our results for anisotropy in polystyrene after normalizing background-subtracted spectra by the CH_3 rocking vibration (1033 cm^{-1}) corresponded very well with previous studies using infrared dichroism (Fig. S6).(30–33) Therefore, we employed a similar normalization protocol for NBR samples. We observed that the CH_2 twisting (tw) vibration (1300 cm^{-1}) showed no anisotropy in strained NBR spectra, and thus the CH_2 tw peak was used as an independent peak for normalization of $A_{\parallel}$ and $A_{\perp}$in all NBR spectra.

We focus on the C=C stretch (1666 cm^{-1}) from the *trans*-1,4-butadiene monomer (marked by letter k in Fig. 3a)(34, 35) and C≡N stretch (2235 cm^{-1}) vibrations in NBR to anisotropy and chain alignment. The C=C backbone and C≡N sidechain group will align (somewhat) parallel and perpendicular to the loading direction, respectively, as chain alignment increases (Fig.3a and Fig. S7). Figure 3b, shows S_{mol} for both vibrations. As expected, we find that S_{mol} (C=C) became more positive and S_{mol} (C≡N) became

more negative with increasing ε_{eng} for all nanocomposite samples. The top and bottom orange boxes in Figures 3b and 3c mark the maximum standard error of the mean (s.e.m.) in S_{mol} (C=C) and S_{mol} (C≡N) from the measurements of the unfilled (but vulcanized) NBR, which never showed a statistically significant S_{mol} value at any ε_{eng} when compared to the S_{mol} (ε_{eng} = 0%).

In the subsequent quantification and discussion of anisotropy, we restrict our attention to the C≡N sidechain group since it is a more sensitive marker of chain alignment. This choice is substantiated by the following reasons. First, from a geometrical standpoint, a fully stretched NBR chain (Fig. 3a) will never show purely unidirectional C=C polarizability along the bond of the *trans*-1-4 butadiene because, by definition, this bond cannot align perfectly to the loading direction. Second, the bonding geometry of C≡N is necessarily orthogonal to the (C-C bonds in the) NBR backbone due the *sp* hybridization of the carbon atom. Therefore, the alignment axes of the polymer backbone and CN stretching polarizability are nearly orthogonal, which will increase the anisotropy of this group compared to the C=C bond when a chain is aligned. Consistent with these arguments, we experimentally observed more S_{mol} (C≡N) data points appearing outside of the orange box compared to S_{mol} (C=C). We note that in addition to the C≡N sidechain, a similarly negative anisotropy was observed for CH_2 groups for the CH_2 symmetric vibration (2846 cm^{-1}), which should also lie orthogonal to the chain backbone (Fig. S8a). Taken together, this underscores the robustness of our measurement protocol and molecular anisotropy measurements.

In Figure 3b, asterisks mark the critical ε_{eng} – defined as the ε_{eng} at which we first observed a statistically significant ($p < 0.05$) increase in S_{mol} (C≡N) compared to S_{mol} (C≡N) at $\varepsilon_{eng} = 0$ for each sample. The most prominent trend observed in Figure 3b is that the critical ε_{eng} required to develop a statistically significant C≡N vibrational anisotropy decreased with increasing Φ. We conclude that adding more fillers (increasing Φ) causes NBR chains to align to a greater extent for a given deformation. For the two nanocomposites with Φ = 14 %, we observed a critical ε_{eng} that was slightly lower for the composite with smaller R_{agg} (Fig. 3b, green) compared to that with increased R_{agg} (Fig. 3b, black); otherwise, the S_{mol} (C≡N) vs. ε_{eng} traces look extremely similar.

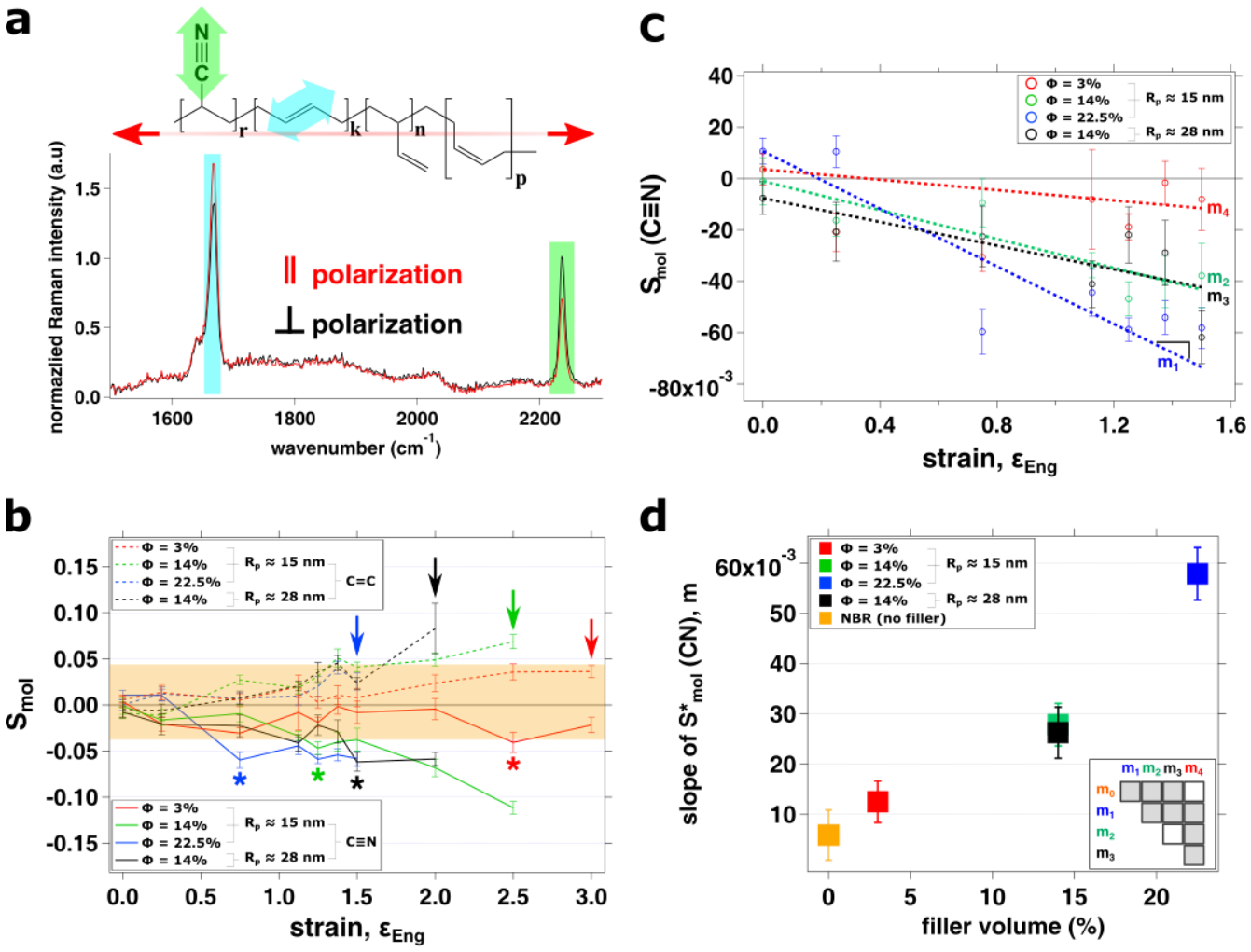

Figure 3. **Polymer anisotropy and molecular spectroscopy of uniaxially stretched nanocomposites.** (a) Molecular structure of an NBR chain aligned to the stretching direction (red line with arrows). Letters *r,k,n,* and *p* represent different monomer units in NBR (see methods). Cyan and green double-sided arrows highlight the direction of the C=C (from *trans*-1,4-butadiene) and C≡N stretching vibrations, respectively. Raman peaks corresponding to these vibrations are highlighted in the example Raman spectra of a stretched (ε_{Eng} = 2.5) nanocomposite (Φ = 14%, R_p = 15 nm). The red and black lines show spectra obtained when the Raman excitation light was parallel and perpendicular to the loading direction, respectively. (b) Vibrational anisotropy (S_{mol}) at increasing strains (ε_{eng}) in different nanocomposites with different amount and R_p fillers. S_{mol} (C=C) from *trans*-1-4 butadiene (1665 cm^{-1}) and S_{mol} (C≡N) (2235 cm^{-1}) stretching vibrations are shown with dashed and straight lines, respectively. Top and bottom orange boxes show the maximum s.e.m. of S_{mol} (C=C, top) and minimum s.e.m. of S_{mol} (C≡N, bottom), respectively, from the neat NBR data. Asterisks indicate ε_{eng} levels where the significant anisotropies ($p < 0.05$) were observed compared to unstrained samples (ε_{eng} = 0) (1-way ANOVA

with Tukey's and Student Newman-Keuls tests). Colored arrows show the largest bearable ε_{eng} before fracture. (c) Linear fits to the S_{mol} (C≡N) between ε_{eng} levels of 0 and 1.5. The slope (m) of NBR without any filler inside (m_0) is shown in Figure S9. Error bars in (b) and (c) are s.e.m. from a minimum of 6 spectra (each for $A_{\parallel}$ and $A_{\perp}$at each ε_{Eng}) from different locations from at least 3 different slices of each nanocomposite. (d) Relation between the slope values and filler amount. Inset shows, statistical differences of each pair of slopes ($p < 0.05$, t-test) in a box chart are shown by grey boxes. Error bars are s.d. from the regression line fits presented in (c).

As a method to compare the trends in Figure 3b, we linearly fit the S_{mol} (C≡N) vs. ε_{eng} for each composite from ε_{eng} = 0 until ε_{eng} = 1.5 (Fig.3c). This range was chosen because ε_{eng} = 1.5 was the highest ε_{eng} from which we were able to collect Raman data from all samples. The slope of each fit, $m = (\Delta S_{mol}) \,/\, (\Delta \varepsilon_{eng})$, is a measure for how increasing ε_{eng} induces C≡N anisotropy, and therefore chain alignment, in the composites. Figure 3d shows that m increases with Φ, and the results from statistical comparison of m from different samples are summarized in the inset; significant differences between two slopes ($p < 0.05$) are shown by grey boxes. All slopes were statistically independent except for those from the composites with Φ = 14%, which again confirms that volume fraction, but not filler size, affects chain alignment.

Since the slope in anisotropy, m, and G_p both vary with Φ, we plotted these variables against one another in Figure 4. This graph clearly shows that these variables are positively correlated, indicating that strain hardening can be predicted by chain alignment and vice versa in our nanocomposites. Previous work has shown that filler size strongly affects reinforcement(22) and strain hardening in semi-crystalline composites;(8) it is therefore surprising that filler size has almost no effect on chain alignment or strain hardening.

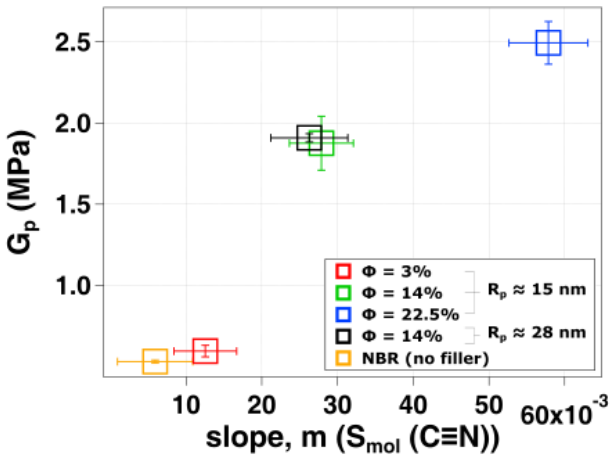

Figure 4. Correlation between strain hardening and chain anisotropy in nanocomposites. Graph shows relation between the $|m|$ from the chain alignment measurements (Fig. 3d) and the strain-hardening modulus (G_p, Fig. 2c) of all samples. Error bars of G_p are s.d (n = 3) and slopes, m are s.d. obtained from the linear regression line fits.

Modeling chain anisotropy in strained nanocomposites

To further interpret the chain alignment experiments, we developed a model for how chain alignment develops under strain and is affected by filler properties. As a starting point, we consider three types of NBR chains in a nanocomposite (Fig. 5a): Type 1) chains that are wrapped around (bound to) the fillers, Type 2) chains that exist within the polymer bulk and not in the vicinity of fillers, and Type 3) chains that exist within space between two fillers – referred to as "bridging" chains. Type 1 chains will necessarily have C≡N side groups that are radially symmetric and will therefore not contribute to S_{mol} (C≡N). From our measurements in unfilled, vulcanized NBR, we empirically found that Type 2 chains generate no detectable anisotropy of C≡N bonds (Fig. S9). This leaves Type 3 bridging chains as the primary contributor to our measured C≡N anisotropy.

We assume that each Type 3 chain contributes a certain amount of Raman signal to $A_\perp$ and $A_\parallel$ – the C≡N vibration Raman intensities acquired orthogonal and parallel to the loading direction – such that

$1 = A_{\parallel} + A_{\perp}$. In the simplest meaningful assumption that each chain has *N* monomers, each with a size *a*, we can write $A_{\perp} \sim \frac{L}{Na}$, where *L* parameterizes the space between fillers. This relation states that the Raman amplitude for C≡N vibrations in a Type 3 chain in the direction orthogonal to the loading direction scales proportionally with distance between fillers and inversely with chain length, which follows intuition for bridging chains. However, $A_{\perp}$ must be constrained because when *L* is greater than *Na* (the contour length of the chain), the anisotropy should no longer increase, and we impose this constraint by writing $A_{\perp} \sim \tanh \frac{2L}{Na}$. The space between fillers $L \sim L_o(1 + \varepsilon_{eng})$, where L_0 is the space between fillers in the unstrained composite, and we assume affine deformation (see Fig. S3). We calculate L_0 using a conservation of volume argument as $L_0 \sim R_{agg}\left[\frac{1-\Phi}{\Phi}\right]^3$, where Φ is volume fraction and R_{agg} is the characteristic filler (aggregate) radius from Figure 1. A schematic for the model is shown in Figure 5a.

With this model defined, we calculated S_{mol} for a single Type 3 chain (S_{mol}^{chain}) and by multiplying this value by N_3 such Type 3 chains in the focal volume, we arrive at the total S_{mol} value, which has the form,

$$S_{mol} = N_3 \cdot \mathrm{S}_{\mathrm{mol}}^{\mathrm{chain}} = N_3 \cdot \frac{1-2\tanh\frac{2L}{Na}}{1+\tanh\frac{2L}{Na}}$$

From our measured aggregate size and fitted lines in Figure 3c, we calculated N_3 and S_{mol}^{chain} as function of ε_{eng}, assuming *Na* = 120 nm for an NBR chain with a molecular weight of 250000 g/mol. There are no other free parameters in this calculation. This model allows us to investigate the mechanism of increasing S_{mol} (C≡N) with ε for the different composites with respect to individual chain anisotropy and number of total contributing Type 3 chains.

Our calculations showed that N_3 and $\left|S_{mol}^{chain}\right|$ increase with ε for all systems and that N_3 was largest at largest Φ whereas $\left|S_{mol}^{chain}\right|$ was smallest at largest Φ (Fig. 5b). Interestingly, at Φ = 14%, we observed that N_3 was larger with smaller R_{agg} (because there are comparatively more bridging chains for greater S_{spe}), whereas $\left|S_{mol}^{chain}\right|$ was larger with larger R_{agg} (because of the larger L_0 between aggregates). Since the total signal is proportional to the product $N_3 \cdot \mathrm{S}_{\mathrm{mol}}^{\mathrm{chain}}$, this model reveals that these two effects must compensate one another.

Figure 5c shows nanocomposite ultrastructure at ε_{eng} = 1.5 based on our model and experimental chain alignment data. Unfilled NBR (orange box, Fig. 5c) only has Type 2 (green) chains due to the absence of fillers. Weak anisotropy could in principle originate from Type 2 chains, but this was undetectable in our spectroscopic measurements. In the presence of the lowest volume fraction fillers (Φ = 3%), Type 3 (red) chains begin to weakly contribute to the measured S_{mol}. Because Φ is relatively low, $L_o \sim Na$ (the contour length of a chain), and the anisotropy of Type 3 *bridging chains* ($\left|S_{mol}^{chain}\right|$) is quite large. However, because Φ = 3%, very few bridging chains exist, i.e. N_3 is small, and the measured S_{mol} is barely detectable.

Samples with Φ = 14% are shown in the black and green boxes in Figure 5c for the samples with large and small R_{agg}, respectively. Larger R_{agg} increases L_o, leading to larger $\left|S_{mol}^{chain}\right|$. However, the nanocomposite with smaller R_{agg} has smaller L_o due to larger S_{spe}, which increases the number of the bridging chains (N_3) in the same volume relative to the sample with larger R_{agg}. These two effects cancel out, resulting in the same S_{mol} for both samples. When Φ = 22.5% (blue box in Fig. 4c), L_o and $\left|S_{mol}^{chain}\right|$ are smallest of all measured nanocomposites, but the number of bridging chains (N_3) is largest since the aggregates are most densely packed (and have the largest S_{spe}), leading to the largest measured chain alignment. These ultrastructure schematics illustrate the compensatory nature between bridging chain alignment and number that vary in opposite ways with respect to surface-to-surface distance of the filler aggregates.

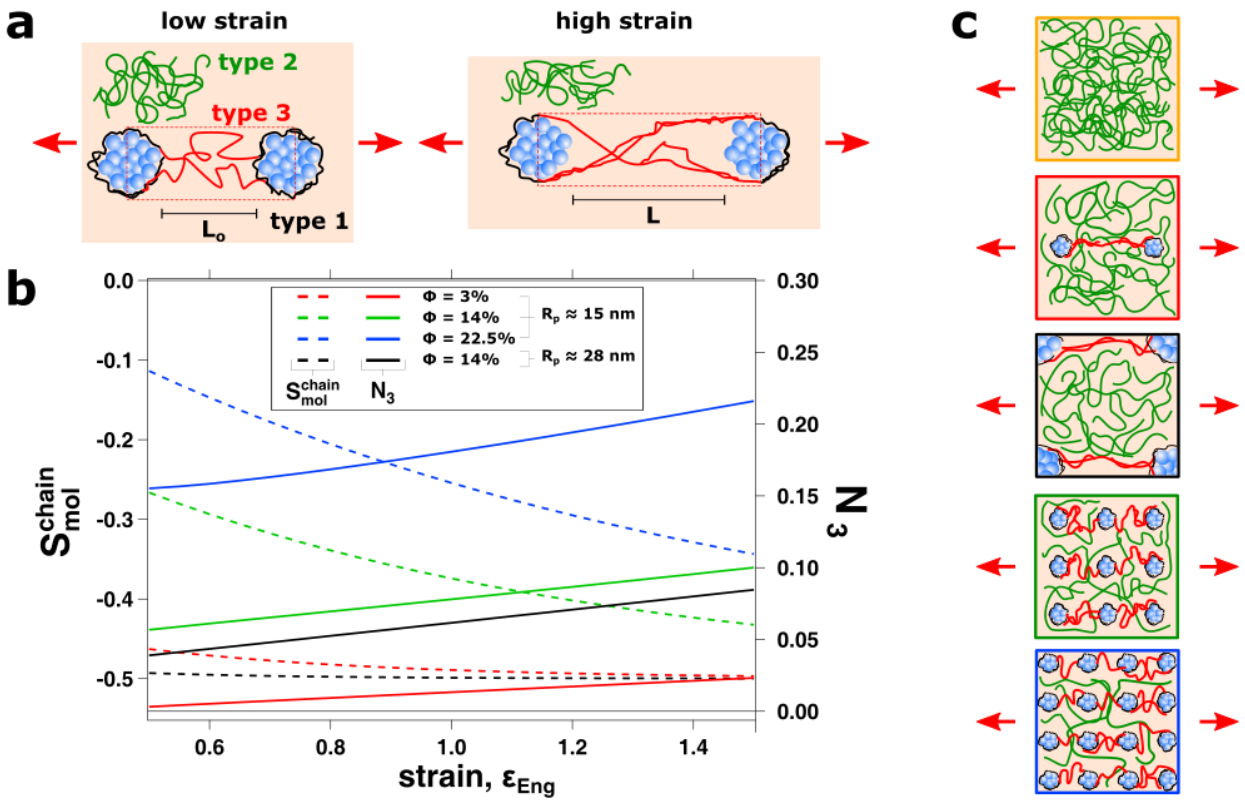

Figure 5. Modeling chain alignment in nanocomposites. (a) Illustration showing the three different type of NBR in a typical nanocomposite structure for our scaling theory at low strain (left) and high strain (right). Type 1 (black) and Type 2 (green) chains represent filler-adsorbed and bulk rubber, respectively. Type 3 (red) chains bridge the filler aggregates to each other and are called "bridging" chains. The bridging region is indicated by the red box with dashed line showing. Under strain Type 1 chains delaminate from particles, enter the bridging region, and convert to Type 3 chains. (b) Graph showing calculated S_{mol}^{chain} (C≡N bonds, dashed lines) and number of Type 3 chains (N_3, solid lines) as a function of ε_{eng} based on the scaling argument presented in the text. S_{mol}^{chain} decreases (becomes more negative) and N_3 increases with ε_{eng}. (c) Schematic illustrations of the predicted ultrastructural features in nanocomposites at ε_{eng} = 1.5. Ultrastructure of neat NBR is illustrated in the orange box. Microstructures sketched in red, green and blue boxes represent the composites including small fillers (R_p ≈ 15 nm) at Φ = 3%, 14% and 22.5%, respectively. Microstructure in black is for Φ = 14% with the larger filler particles (R_p ≈ 28 nm). Color codes of different types of polymer chains (Type 1, Type 2, and Type3) are the same as those in (a). The L_o and R_{agg} represented in each illustration are scaled realistically, under the assumption that aggregates are perfectly distributed in a cubic lattice.

Relation between nancomposite anisotropy and strain hardening

Our work shows how strain hardening and strain-induced chain alignment are strongly correlated and vary with Φ alone, independent of nanofiller ultrastructure. Within the context of our model, the mechanism underlying how increasing ε increases $\left|S_{mol}^{chain}\right|$ and N_3, thereby increasing S_{mol} follows the forthcoming logic. I) L increases with strain, increasing $\left|S_{mol}^{chain}\right|$ until it reaches a maximum (-0.5), and II) conversion of Type 1 chains into Type 3 chains via shear-induced delamination of Type 1 chains from the filler surface (Fig. 5a, red dotted boxes). Conversion of "slippery" adsorbed (Type 1) chains into Type 3 chains has been shown, specifically in samples (nearly identical to ours) where limited interaction between the polymer and fillers is present.(18, 36) While it is, in principle, possible to disrupt filler aggregates with increasing tensile strain, which would have a similar effect as delamination, scanning electron micrograph images of 150% strained nanocomposite samples show no such effects (Fig. S10).

Recalling again the results of Jancar *et al*. where PMMA microcomposites showed almost no strain hardening compared to nanocomposites at the same Φ, this raises an interesting question. Over what length scale do Type 3 chains exist, and therefore contribute tangible chain alignment, in composite systems? Looking at our data from unfilled and Φ = 3% nanocomposites, we conjecture that detectable chain alignment only occurs when $L_o \sim Na$. In microcomposites, $L_o \sim$ µm (>> Na of the PMMA), whereas $L_o \sim Na$ in nanocomposites. Therefore, the microcomposite case approaches that of a vanishingly low Φ in nanocomposites, where almost no Type 3 chains exist, which results in minimal chain alignment and therefore minimal strain hardening.

Conclusion

The effect of nanofiller size and amount on non-linear strain hardening of cross-linked elastomers (T_g ~ -30 °C) was quantified here for various NBR nanocomposites. By measuring both their mechanical strain hardening and chain alignment with increasing tensile strain, we show that both the strain-hardening modulus and chain alignment in NBR composites only depend on filler amount and were independent of the filler size. Furthermore, these two variables were positively correlated highlighting the relation between them. Using a simple scaling argument, we arrive at a mechanism for chain alignment that only depends on filler volume fraction via a compensatory effect between individual chain alignment and number of (bridging) chains aligning to the load. While our work highlights the importance of chains bridging filler aggregates over a length scale comparable with the contour length of a chain, Baeza *et al*. recently related the complex linear elasticity in nanocomposites to network formation among overlapping tightly bound chains in close proximity (~ nm) to filler surfaces.(37) Along with our results showing that nonlinear elasticity of nanocomposites is insensitive to filler size, this underscores the different physico-chemical origin of the linear and nonlinear elasticity in these materials. This suggests that nanocomposite design can be optimized in a two-tiered process wherein one tunes the strain hardening properties and mechanical reinforcement independently by: 1) choosing an amount of nanofillers to target a specific nonlinear strain hardening response and 2) selecting a particular size of nanofillers to obtain a desired reinforcement.

Materials and Methods

Nanocomposite formulations and dipole moments of the rubbers

SiO_2 (primary particle sizes, R_p are ca. 15 nm, 20 nm and 28 nm) / Acrylonitrile Butadiene Rubber (NBR, M_w = 250000 g/mol, glass transition temperature, T_g ≈ -36 °C (see Fig. S5)) nanocomposites were produced at SKF Elgin, USA.(38) In terms of per hundred rubber units (PHR), the filler amounts in the NBR composites can be re written as 10 PHR (Φ = 3%), 30 PHR (Φ = 8.2%), 50 PHR (Φ = 14%) and 90 PHR (Φ = 22.5%). Other fundamental ingredients and their amounts in all NBR systems are: NBR (100 PHR), stearic acid (1 PHR), ZnO (9 PHR), rubber activator (2.5 PHR), sulphur (1.2 PHR) and curing agent (2.5 PHR). Besides of the volume and R_p of the fillers, all the other synthetic parameters were kept the same. Unfortunately, further mixing and synthetic details of the NBR composites cannot be provided in here. Briefly, NBR rubber synthesized as nitrile elastomers which are synthesized via emulsion polymerization of 1,3-butadiene and acrylonitrile (ACN) with the monomer ratio of 72:28.

Electron Microscopy Imaging and Image Processing

Transmission electron microscopy (TEM)

TEM imaging was performed after sectioning the nanocomposites to a thickness of ca. 50 nm by ultracryotome (LEICA EM UC6, Wetzlar, Germany) at −60 °C using a diamond knife (Cryotome ultra 35°, Hatfield, USA). The magnification was set to 5000X, and images were obtained with constant electron beam intensity and an acceleration voltage of 120 kV on a JEOL electron microscope (JEOL JEM 1400, Eching).

Scanning electron microscopy of stretched samples

Prior to the imaging, nanocomposite samples where were cut to 10 µm thick sections with ultracryotome at −60 °C. These slices were stretched to ε_{Eng} = 1.5 and fixed on the silicon wafer with using super glue (Loctite, 528). The magnification was set to 5000X, and images were acquired with a constant electron beam intensity and an acceleration voltage of 120 kV on a LEO 1530 Gemini microscope (Leo Electron Microscopy Ltd., Zeiss, Oberkochen, Germany).

Electron microscopy image processing

For TEM (8-bit images), the following image processing routine was used to find the average aggregate size (R_{agg}) of nanocomposites. More than 4000 aggregates were imaged per sample from different regions of at least two sections from each composite formulation. Image analyses of electron microscope micrographs were done by using a thresholding routine in ImageJ to differentiate silica from the background polymer and obtain an area (in μm^2) for each individual aggregate. Details of the thresholding steps of TEM images are explained at length in reference 36.(23) Aggregate areas for each composite is shown in Figure S1, and the cumulative distribution function of each histogram (red dashed curves in Fig. S1) is also shown. The characteristic aggregate area was determined by discarding those aggregates in the 90th – 100th percentile of the histogram and performing a weighted average of the remaining samples. R_{agg} was then calculated assuming a circular shape.

For stretched samples measured with scanning electron microscopy (8-bit) images, ImageJ also used to process the images; however the threshold parameters were set differently than for TEM. The threshold was set to 105 and the circularity were used between 0.1 – 1.0. Starting the circularity from 0.1 helped us to avoid of counting highly charged areas around the voids in stretched samples as aggregate. For these images, all the aggregates averaged and R_{agg} was calculated assuming a circular shape.

Mechanical measurements and mechanical statistics

Uniaxial tensile measurements of nanocomposites were done by using an Instron Universal Testing Machine (Instron 6022, Darmstadt). Samples were cut into a dumbbell shape (length ≈ 1 cm, thickness ≈ 0.2 cm, width ≈ 0.18 cm) and they were clamped to the tensile testing device by applying 5 bar of clamping pressure. No pre-strain was applied and strain rate was kept 100 mm/sec for each measurement. Mechanical tests were stopped manually after the fracture of the composite. Three different stress (σ)- strain (ε) measurements were performed from each type of nanocomposite in order to have statistically consistent mechanical results. The engineering (or nominal) stress (σ_{Eng}) – engineering strain (ε_{Eng}) curves of different NBR formulations were derived after mechanical tests of the composites by following equations,

$$\sigma_{Eng} = P\ (applied\ load)/A_0(initial\ cross-sectional\ area))$$

$$\varepsilon_{Eng} = \Delta l\ (change\ in\ lenght)/l_0(initial\ lenght)$$

To the best of our knowledge, we can assume that the volume of the composites are constant during the deformation, and thus have *Poisson's ratio* of 0.5.(4) In constant volume, true stress (σ_{True}) – true strain (ε_{True}) curves of all the nanocomposite samples were calculated using following equations,

$$\sigma_{True} = \sigma_{Eng}(\varepsilon_{Eng} + 1)$$

$$\varepsilon_{True} = \ln(\varepsilon_{Eng} + 1)$$

Anisotropy measurements by Raman Micro-spectroscopy

All the nanocomposite samples were sectioned in ca. 15 µm thicknesses by using low profile diamond blade (C.L. Sturkey Inc., Lebanon, USA) in a cryotome device (cryostat – MTC, Slee medical, Mainz, Germany) at -27 °C. These thin films were then glued on stretching brass pieces of a house –build tensile device by using super glue (Loctite 528). The gap distance between these brass blocks can be changed with in sub-micron steps by mounting a motorized actuator (THORLABS Z825B, New Jersey, USA) to the tool and this distance between gaps used for defining the strain levels (Figure S11). Strain rate and acceleration were kept 0.025 mm/sec and 0.025 mm/sec^2, respectively, for all the stretching steps between polarized Raman measurements.

At each strain level, Raman spectra of the samples were recorded with an uRaman module having a 633 nm excitation (TechnoSpex) using a (50X, 0.75 NA, Olympus). Samples at different draw ratios were placed under the constant polarized incident Raman laser with ~ 40 mW power. The angle between the drawing direction and the polarization direction was changed by rotating the sample (0° and 90°) and no analyser were placed before the detector. From each polarization angle and level of stretching, we recorded at least 6 different spectra from at least 3 different slices from each composite. Each spectrum was measured with an integration time of 24 sec.

Statistics

In order to discuss the statistical differences of the R_{agg} between different nanocomposites and G_p, we performed ANOVA package in IgorPro by using the Tukey test. Differences were considered significant when ($p<0.05$).

For S_{mol} Tukey and Student Newman-Keuls tests (SNK) were performed using IgorPro for all samples. We used ANOVA and tested the significance in S_{mol} at each strain compared to the same sample at S_{mol} at $\varepsilon=0$. The value was considered statistically different when we observed a significant difference from both tests.

Significant differences between the linear slopes of S_{mol} (C≡N) data between 0 and 1.5 strain levels of different SiO_2 / NBR samples were tested by following steps. First, all measured S_{mol} data for a given sample (not only averages) was fit with a line in Igor Pro from $\varepsilon = 0$ until $\varepsilon = 1.5$ with the intercept locked to the mean S_{mol} at $\varepsilon=0$. In order to compare two different slopes from two different samples we assume that all the slopes follow t distribution (2-tailed).

$$t = \frac{b_1 - b_2}{\sqrt{s_{b1}^2 + s_{b2}^2}}$$

Where b_1 and b_2 refer to the slopes of the S_{mol} from sample 1 and sample 2, respectively. s_b^2 values show the standard errors of these slopes. b and s_b values were obtained as the results of the linear fitting in IgorPro. t-value then compared to the critical value of the t-distribution of cumulative distribution function in literature(39) by using $v = n_1 + n_2 - 4$ degrees of freedom. n show the total number of S_{mol} values between 0 and 1.5 strain levels. The significance between sample 1 and sample 2 is decided by finding the probability, p value in the distribution function table and statistical significance of the slopes is confirmed if $p<0.05$ according to 2-tailed t-test.(39)

Acknowledgements

We acknowledge Florian Gericke, Walter Scholdei, Jürgen Worm, and Marc-Jan van Zadel for excellent technical support with building the spectroscopy setup. Andreas Hanewald and Sabine Pütz assisted with measurements of strain hardening and T_g, Johannes Hunger for stimulating discussions, and William Rock helped with analytical software development. This work is part of the research programme 'Understanding the visco-elasticity of elastomer based nanocomposites' (11VEC01) of the' Stichting voor Fundamenteel Onderzoek der Materie (FOM)', which is financially supported by the' Nederlandse Organisatie voor Wetenschappelijk Onderzoek (NWO).

References

1. Carey BJ, Patra PK, Ci L, Silva GG, Ajayan PM (2011) Observation of dynamic strain hardening in polymer nanocomposites. *ACS Nano* 5(4):2715–2722.
2. Huang Y, Paul DR (2007) Effect of MolecularWeight and Temperature on Physical Aging of ThinGlassy Poly(2,6-dimethyl-1,4-phenylene oxide) Films. *J Polym Sci Part B Polym Phys* 45(April):1390–1398.
3. Jancar J, Douglas J, Starr F (2010) Current issues in research on structure–property relationships in polymer nanocomposites. *Polymer (Guildf)* 51:3321–3343.
4. Fried JR (2003) *Polymer Science and Technology* (Prentice Hall, NJ).
5. Riande E, Diaz-Calledja R, Prolongo MG, Masegosa RM, Salom C (2000) *Polymer Viscoelasticity: Stress and Strain in Practice* (Marcel Dekker AG, New York and Basel).
6. Haward RN (1993) Strain Hardening of Thermoplastics. *Macromolecules* 26:5860–5869.
7. Na B, et al. (2007) Inverse temperature dependence of strain hardening in ultrahigh molecular weight polyethylene: Role of lamellar coupling and entanglement density. *J Phys Chem B* 111(46):13206–13210.
8. Jancar J, Hoy RS, Lesser AJ, Jancarova E, Zidek J (2013) Effect of Particle Size, Temperature, and DeformationRate on the Plastic Flow and Strain Hardening Response of PMMA Composites. *Macromolecules* 46(23):9409–9426.
9. PUKANSZKY B (1990) Influence of interface interaction on the ultimate tensile properties of polymer composites. *Composites* 21(3):255–262.
10. Costa P, et al. (2012) Mechanical, electrical and electro-mechanical properties of thermoplastic elastomer styrene–butadiene–styrene/multiwall carbon nanotubes composites. *J Mater Sci*:1172–1179.

11. Riggleman RA, Toepperwein G, Papakonstantopoulos GJ, Barrat J-L, de Pablo JJ (2009) Entanglement network in nanoparticle reinforced polymers. *J Chem Phys* 130(24):244903.

12. Jiang F, et al. (2015) Combination of magnetic and enhanced mechanical properties for copolymer-grafted magnetite composite thermoplastic elastomers. *ACS Appl Mater Interfaces* 7(19):10563–10575.

13. Jiang F, Zhang Y, Fang C, Wang Z, Wang Z (2014) From soft to strong elastomers: the role of additional crosslinkings in copolymer-grafted multiwalled carbon nanotube composite thermoplastic elastomers. *RSC Adv* 4(104):60079–60085.

14. Pei A, Malho JM, Ruokolainen J, Zhou Q, Berglund LA (2011) Strong nanocomposite reinforcement effects in polyurethane elastomer with low volume fraction of cellulose nanocrystals. *Macromolecules* 44(11):4422–4427.

15. Ha YH, Thomas EL (2002) Deformation behavior of a roll-cast layered-silicate/lamellar triblock copolymer nanocomposite. *Macromolecules* 35(11):4419–4428.

16. Bokobza L (2001) Filled elastomers : a new approach based on measurements of chain orientation. *Polymer (Guildf)* 42:5415–5423.

17. Bokobza L, et al. (2002) Effects of Filler Particle/Elastomer Distribution and Interaction on Composite Mechanical Properties. *Chem Mater* 14(1):162–167.

18. Wang Z, Liu J, Wu S, Wang W, Zhang L (2010) Novel percolation phenomena and mechanism of strengthening elastomers by nanofillers. *Phys Chem Chem Phys* 12(12):3014–3030.

19. Bistričić L, Leskovac M, Baranović G, Blagojević SL (2008) Mechanical properties and linear infrared dichroism of thin films of polyurethane nanocomposites. *J Appl Polym Sci* 108(2):791–803.

20. Treloar LR. (1975) *The Physics of Rubber Elasticity* ed Treloar LR. (Oxford University Press, Oxford).

21. Rubinstein M, Colby RH (2003) *Polymer physics (Chemistry)* (Oxford University Press, Oxford).

22. Mermet-Guyennet MRB, et al. (2015) Size-dependent reinforcement of composite rubbers. *Polymer (Guildf)* 73:170–173.

23. Varol HS, et al. (2015) Multiscale Effects of Interfacial Polymer Confinement in Silica Nanocomposites. *Macromolecules* 48(21):7929–7937.

24. Mooney M (1940) A theory of large elastic deformation. *J Appl Phys* 11(9):582–592.

25. Haward RN (1997) *The physics of glassy polymers* (Springer Netherlands, Dordrecht). 2nd Ed.

26. Fang C, et al. (2015) Fabrication of Copolymer-Grafted Multiwalled Carbon Nanotube Composite Thermoplastic Elastomers Filled with Unmodified MWCNTs as Additional Nanofillers to Significantly Improve Both Electrical Conductivity and Mechanical Properties. *Ind Eng Chem Res* 54(50):12597–12606.

27. Ward IM, Sweeney J (2012) *Mechanical properties of solid polymers* (John Wiley & Sons, Chichester). 3rd Ed.

28. Lin Y-H (2011) *Polymer viscoelasticity : basics, molecular theories, experiments and simulations* (World Scientific, Singapore). 2nd Ed.

29. Richard-Lacroix M, Pellerin C (2013) Accurate new method for molecular orientation quantification using polarized raman spectroscopy. *Macromolecules* 46(14):5561–5569.

30. Keplinger T, et al. (2015) A versatile strategy for grafting polymers to wood cell walls. *Acta Biomater* 11:256–63.

31. Prasertsri S, Lagarde F, Rattanasom N, Sirisinha C, Daniel P (2013) Raman spectroscopy and thermal analysis of gum and silica-filled NR/SBR blends prepared from latex system. *Polym Test* 32(5):852–861.

32. Prakanrat S, Phinyocheep P, Daniel P (2009) Spectroscopic Investigation of Polystyrene Surface Grafting on Natural Rubber. *Appl Spectrosc* 63(2):233–238.

33. Bruckmoser K, Resch K, Kisslinger T, Lucyshyn T (2015) Measurement of interdiffusion in polymeric materials by applying Raman spectroscopy. *Polym Test* 46:122–133.

34. Siesler HW, Holland-Moritz K (1980) *Infrared and Raman spectroscopy of polymers* (Marcel Dekker, New York and Basel).

35. Bower DI, Maddams MF (1992) *The Vibrational Spectroscopy of Polymers* eds Cahn RW, Davis EA, Ward IM (Cambridge University Press, Cambridge).

36. Kilian HG, Strauss M, Hamm W (1994) Universal Properties in Filler-Loaded Rubbers. *Rubber Chem Technol* 67(1):1–16.

37. Baeza GP, et al. (2016) Network dynamics in nanofilled polymers. *Nat Commun* 7:11368.

38. de Castro JG, et al. (2015) Nonmonotonic fracture behavior of polymer nanocomposites. *Appl Phys Lett* 106(22):221904.

39. Glantz S (2012) *Primer of Biostatistics, Seventh Edition* (McGraw-Hill Education / Medical, New York). 7th Ed.

Supporting Information

Nanoparticle amount, and not size, determines chain alignment and nonlinear hardening in polymer nanocomposites

H. Samet Varol [a], Fanlong Meng [b], Babak Hosseinkhani [d], Christian Malm [a], Daniel Bonn [e], Mischa Bonn [a], Alessio Zaccone [b,c], Sapun H. Parekh [a]

[a] Department of Molecular Spectroscopy, Max Planck Institute for Polymer Research, Mainz, Germany

[b] Cavendish Laboratory, University of Cambridge, CB3 0HE Cambridge, U.K.

[c] Department of Chemical Engineering and Biotechnology, University of Cambridge, CB2 3RA Cambridge, U.K.

[d] SKF Engineering & Research Center, Nieuwegein, The Netherlands

[e] Institute of Physics, University of Amsterdam, Amsterdam, The Netherlands.

Corresponding Author

Sapun H. Parekh

Address: Molecular Spectroscopy Department, Max Planck Institute for Polymer Research

Ackermannweg 10, 55128 Mainz (Germany)

E-mail address: parekh@mpip-mainz.mpg.de

Supporting Methods

Thermal analysis. Differential scanning calorimetry (DSC) measurements were done by operating a DSC 822 (Mettler Toledo) under nitrogen in order to calculate glass-transition temperature (T_g) of nanocomposites and rubber samples with and without vulcanization. ~ 10 mg from each sample placed in sample pans, and DSC curves were obtained after three cycles of measurements between -100°C and +200 °C with a temperature rate of 10 K min^{-1}.

Raman micro-spectroscopy of polystyrene. Polystyrene (PS) slides ((T_g ≈ 100 °C, 1 mm x 25 mm x 75 mm), Nalge Nunc™ Int., Rochester, NY, USA) were first fixed in our stretching stage using clamps. The stage was then placed on top of a heating plate, and the temperature was monitored with a thermo-couple in contact with the PS surface. When the temperature of the PS slide reached to ~ 120 °C and was stable, the PS slide was stretched to the desired strain. Immediately after stretching, the film was immersed in ice water mixture for one minute. After drying, polarized Raman spectra of stretched PS films were recorded using the same measurement parameters as used for the nanocomposites.

Supporting Figures

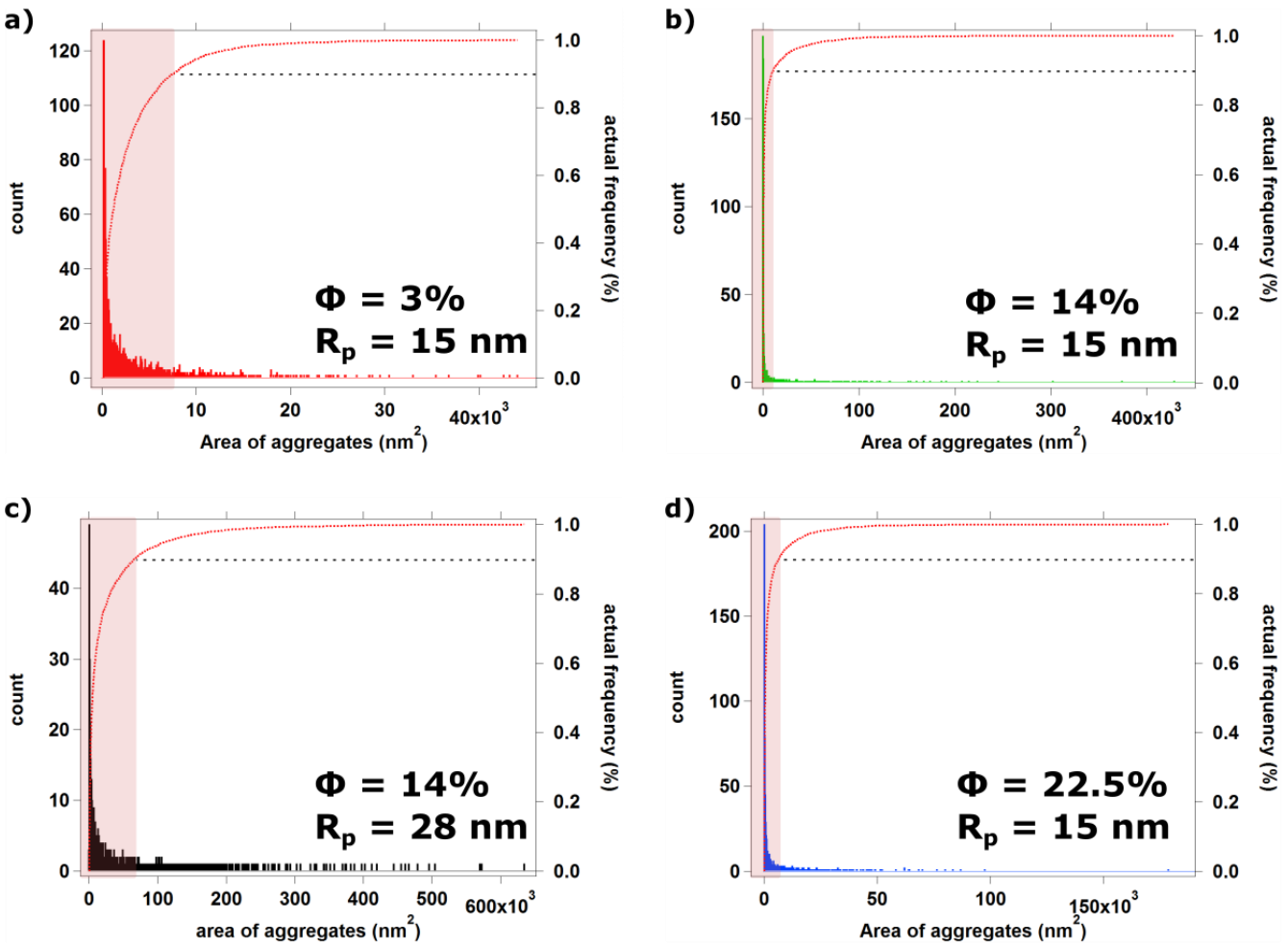

Figure S1. Histograms showing aggregate area sizes in different NBR nanocomposites including various nanofiller particle sizes (R_p) and volume (Φ). Cumulative distribution functions derived from each of these histograms are shown from 0% frequency until 100% frequency (right y-axis) by red dashed lines. Black dashed lines mark the 90th percentile of aggregates, and all aggregates from 0-90th percentile, denoted by the bars in the shaded area (red) in each histogram, were used to calculate the average aggregate area. The 90th -100th percentile in the cumulative distribution functions were discarded.

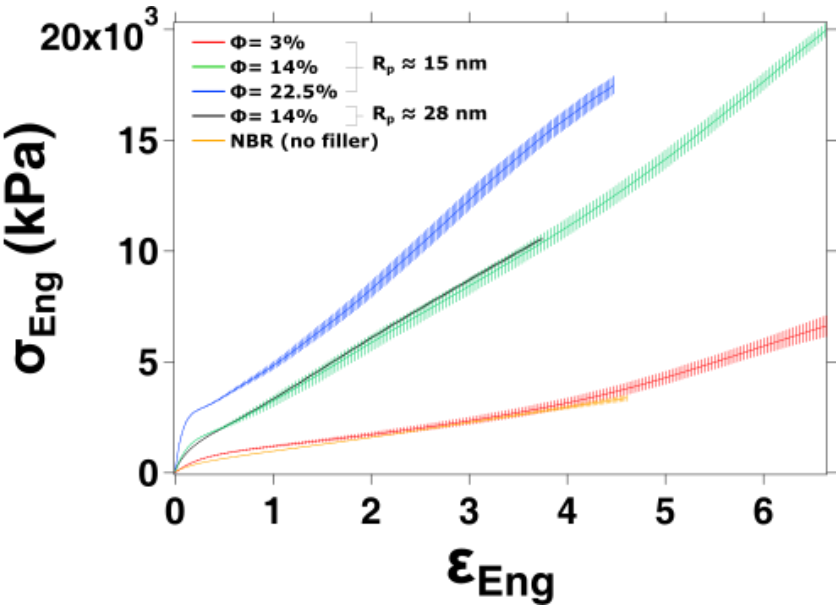

Figure S2. Engineering stress (σ_{Eng}) – engineering strain (ε_{Eng}) curves of neat NBR and NBR nanocomposites including different amount and size of fillers. Error bars are standard deviation (s.d.) from measurements of three slices from the same composite slab.

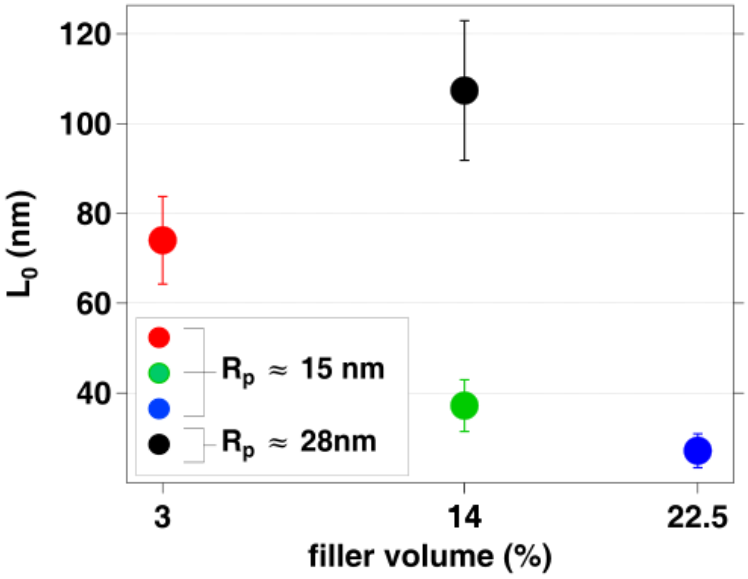

Figure S3. Surface-to-surface distance, $L_0 \sim R_{agg}\left[\frac{1-\Phi}{\Phi}\right]^3$ between aggregates in different NBR nanocomposites. In the formula, R_{agg} is the average aggregate size and Φ is the filler volume. Error bars are derived from standard error of the mean (s.e.m.) of the aggregate size distribution.

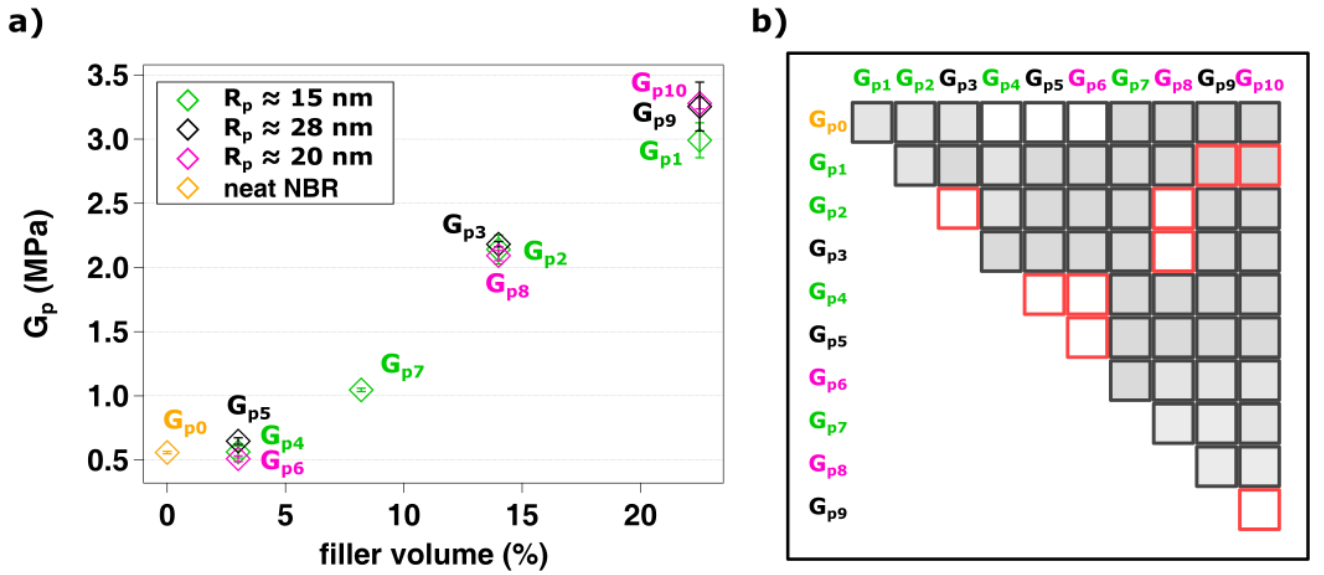

Figure S4. (a) Strain hardening modulus (G_p) of all the NBR nanocomposites and neat NBR derived from Gaussian plots as explained in the main text (Fig. 2). G_p of each sample is labelled using different number and colors. (b) Box chart showing the significant differences ($p < 0.05$) between each pair of G_p by grey filled boxes (1-way ANOVA with Tukey's). Error bars in a are s.d. from measurements of three slices from the same composite slab.

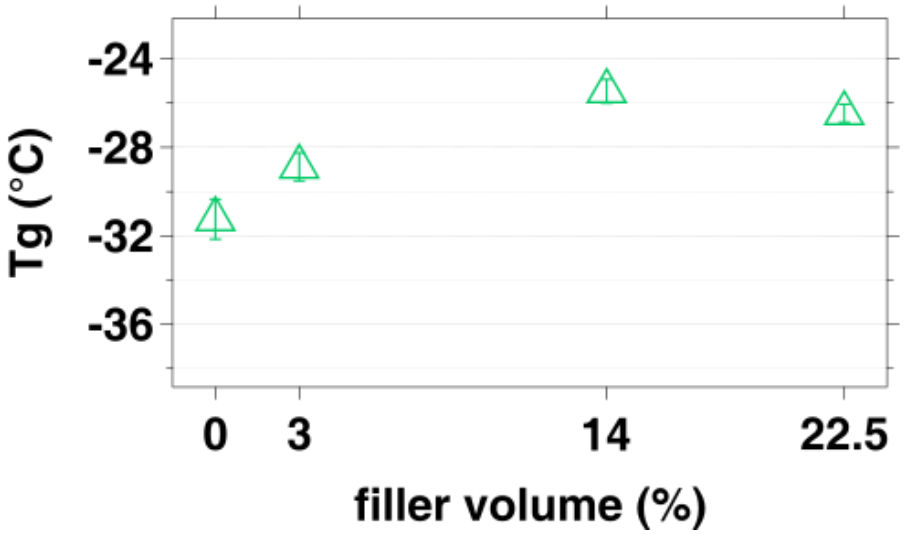

Figure S5. Glass transition temperature (T_g) of neat NBR and NBR nanocomposites including different amount but the same size ($R_p \approx 15$ nm) of fillers. Error bars are s.d. from 3 heating cycles on a single sample from each formulation.

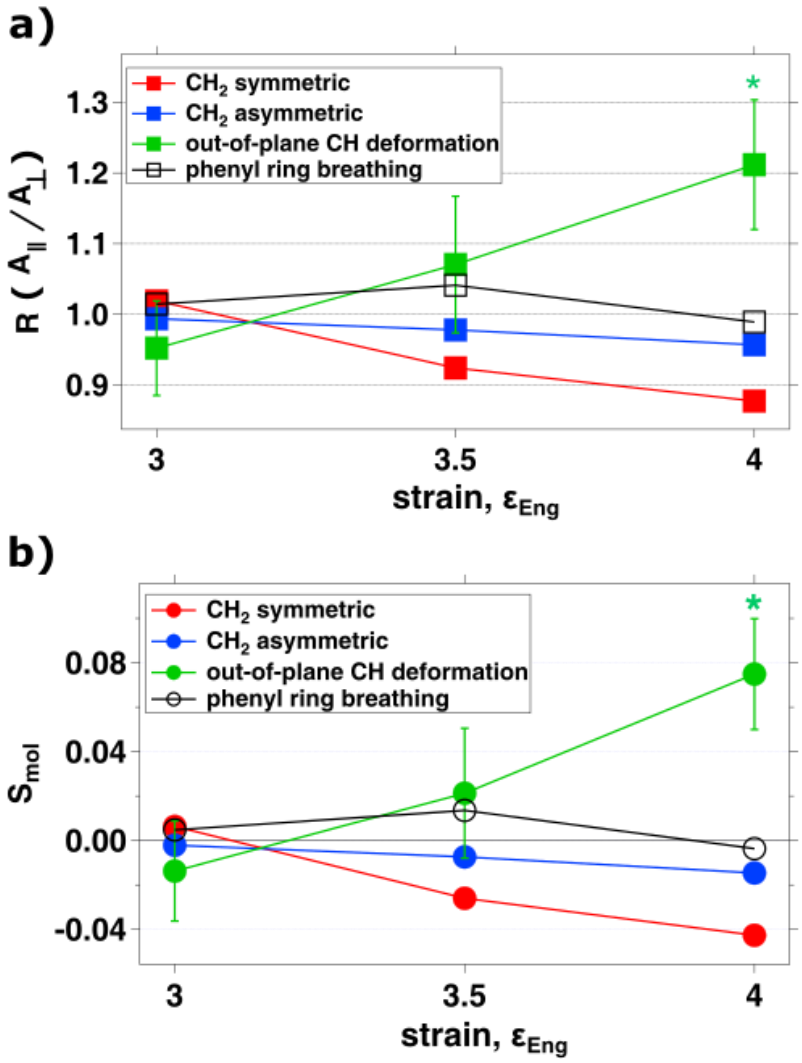

Figure S6. Anisotropy of polystyrene (PS) film at increasing engineering strain (ε_{Eng}) shown as (a) dichroic ratio, *R*, which was obtained from the ratio of the indicated Raman peak intensities in normalized Raman spectra (normalization peak is CH_3 rocking, 1033 cm^{-1}). $R = A_{||} / A_{\perp}$ where $A_{||}$ was the normalized Raman intensity when the stretching direction and excitation laser were parallel and $A_{\perp}$ was the normalized Raman intensity when the stretching direction and excitation laser were perpendicular. (b) Anisotropy of PS vibrations shown by S_{mol} (as in the main text). Significant anisotropy ($p < 0.05$) compared to the *R* and S_{mol} of PS film at $\varepsilon_{Eng} = 0$ is indicated by using asterisk (1-way ANOVA with Tukey's and Student Newman-Keuls tests). Error bars in both plots bars are s.e.m. from measurements three different sections from the same PS slide that were stressed to the indicated value.

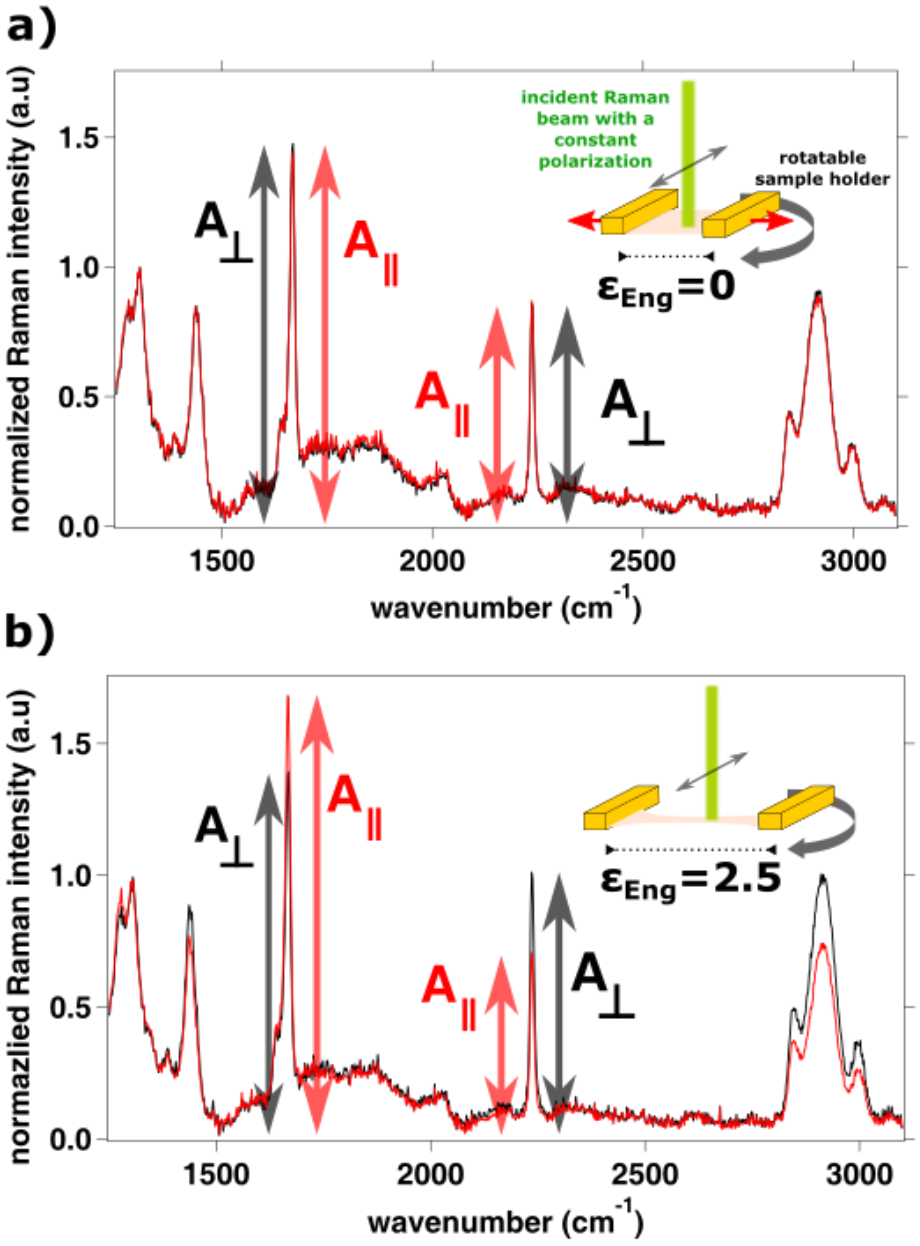

Figure S7. (a) Normalized Raman spectra of NBR nanocomposite (Φ = 14% and R_p = 15 nm) at (a) ε_{Eng} = 0 and (b) ε_{Eng} = 2.5 measured with the excitation laser polarization parallel (red) and perpendicular (black) to the loading direction. Insets illustrate the experimental laser polarization (double-headed arrow) and geometry of polarized Raman measurements. In (a) and (b), amplitude of characteristic Raman peaks are shown by red and black arrows next to the characteristic peaks of C=C (1666 cm^{-1}) and C≡N (2235 cm^{-1}).

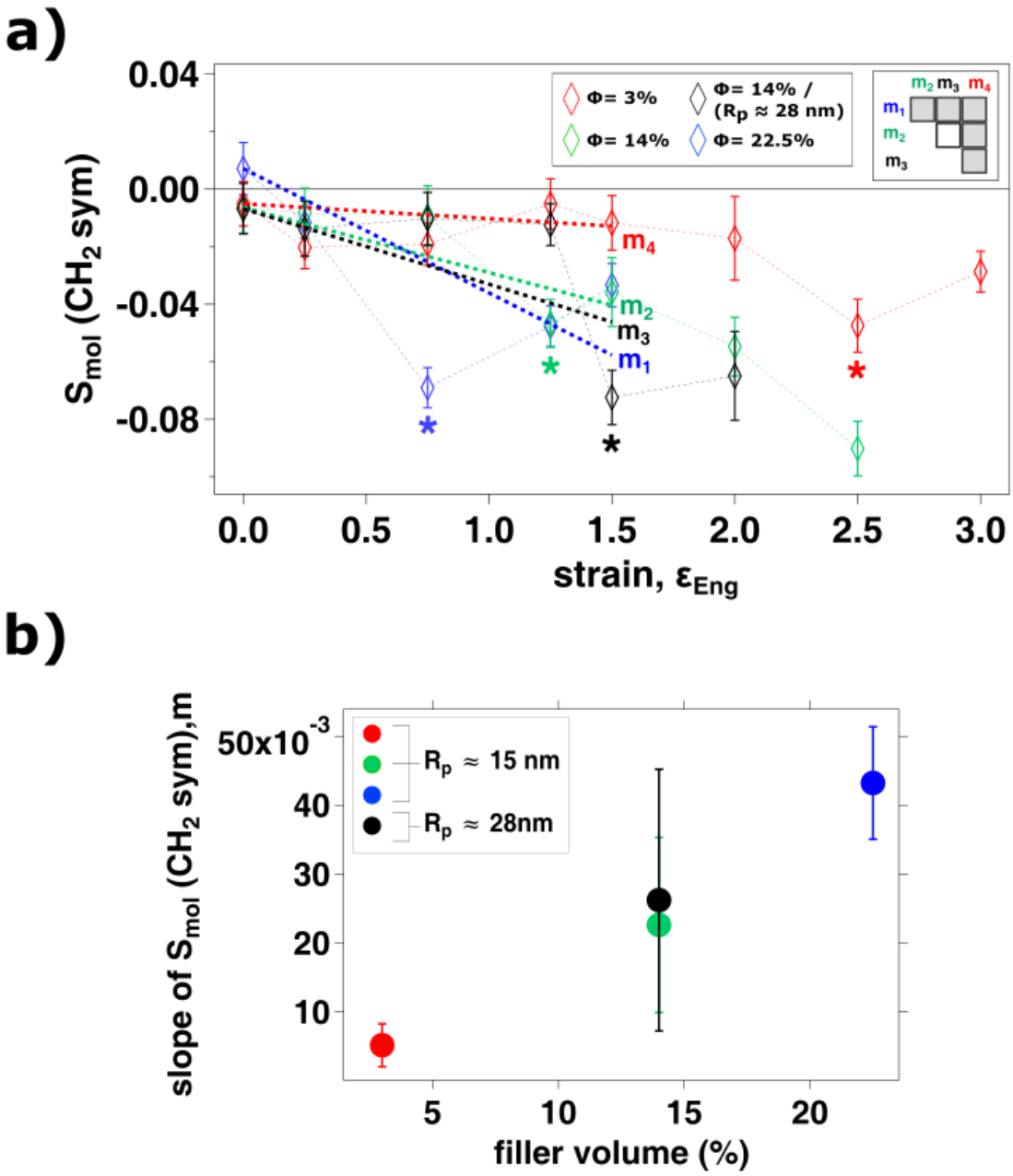

Figure S8. (a) S_{mol} (CH_2 sym, 2846 cm^{-1}, see Figure S7) in NBR composites with increasing strain. Asterisks shows the first significant S_{mol} change compared to the S_{mol} at relaxed state. Dashed lines represents the linear fit of S_{mol} (CH_2 sym) of different samples between relaxed state and ε_{Eng} = 1.5. Statistical comparison (t-test) summary of these slopes are shown in the box chart as an inset. Filled boxes represent the significant difference (p < 0.05) between two regression lines (slopes). (b) The slope amplitudes shown versus filler volume. Error bars in (a) are s.e.m. from a minimum of 6 spectra (each for A_∥ and A_⊥at each ε_{Eng}) from different locations from at least 3 different slices of each

nanocomposite. Error bars in (b) are s.d. from the linear fitting.

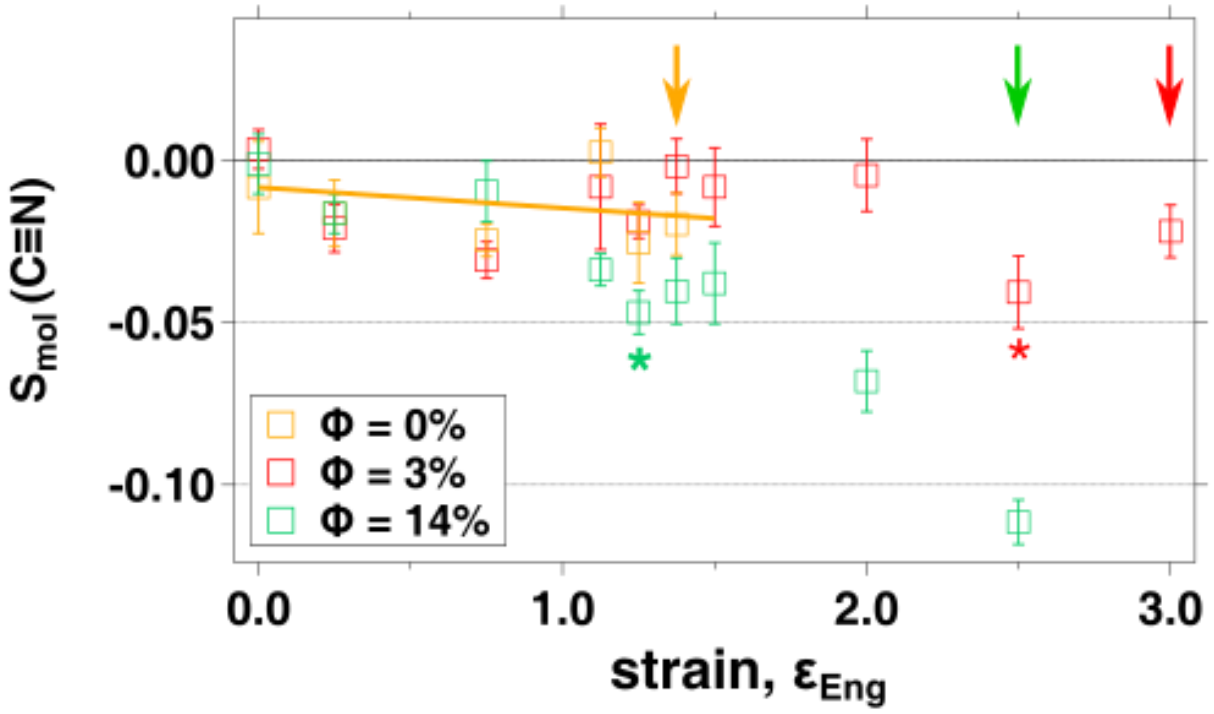

Figure S9. S_{mol} (C≡N) from neat NBR (Φ = 0%) and NBR nanocomposites including Φ = 3% and Φ = 14% fillers (R_p ≈ 15 nm) inside at increasing strain. The largest strain before fracture is shown by different color arrows for each sample. Error bars in (a) are s.e.m. from a minimum of 6 spectra (each for A_∥ and A_⊥at each ε_{Eng}) from different locations from at least 3 different slices of each nanocomposite.

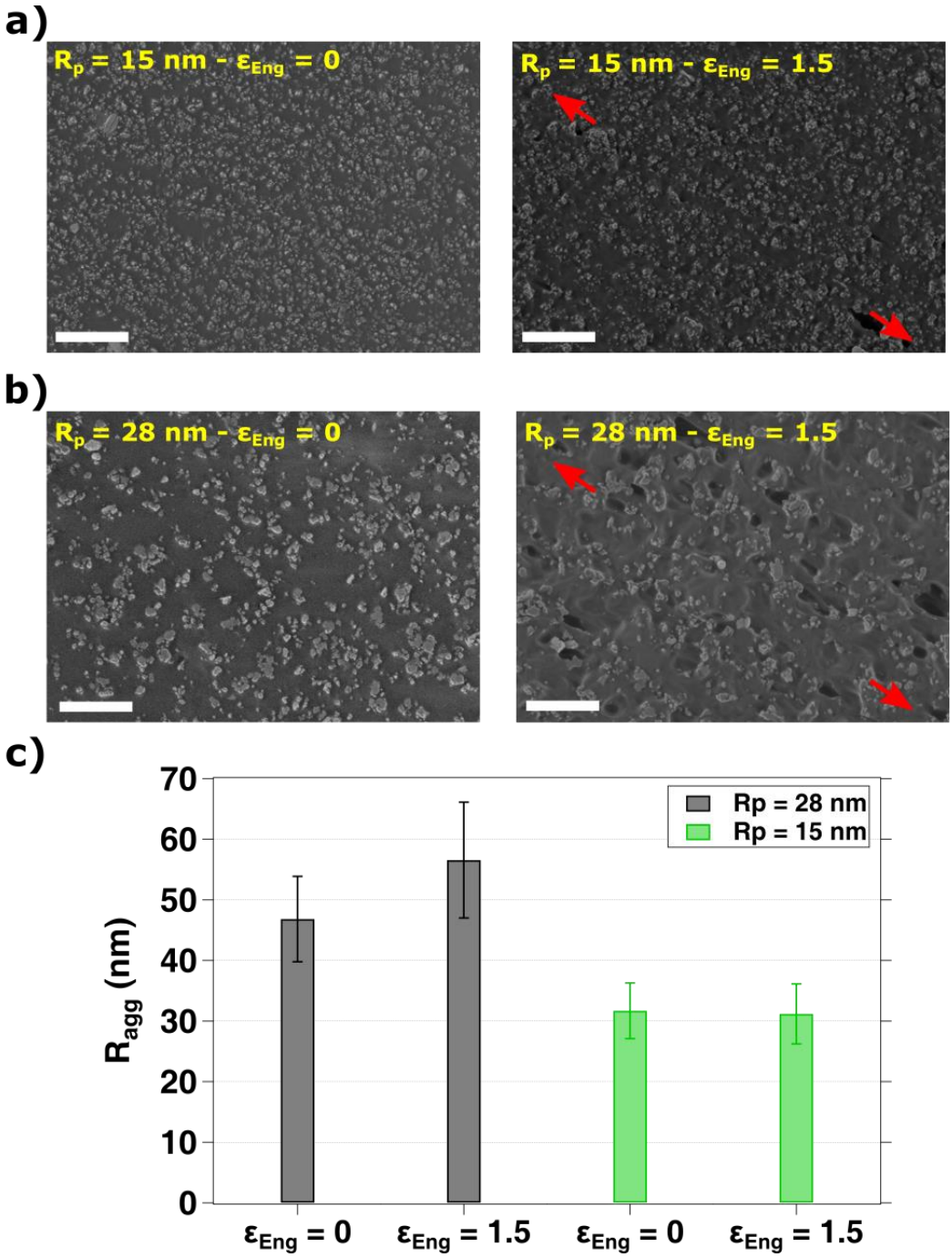

Figure S10. (a) Scanning electron microscope images of NBR nanocomposites (Φ = 14%) including fillers with R_p of (a) 15 nm and (b) 28 nm. In (a) and (b) images in the left and right columns were taken before (ε_{Eng} = 0) and after stretching (ε_{Eng} = 1.5), respectively. Direction of the stretching is shown by red arrows. Scale bars are 1 µm. (c) Average aggregate size (R_{agg}) of the samples shown in (a) and (b). Error bars are s.e.m. from measurements on different samples.

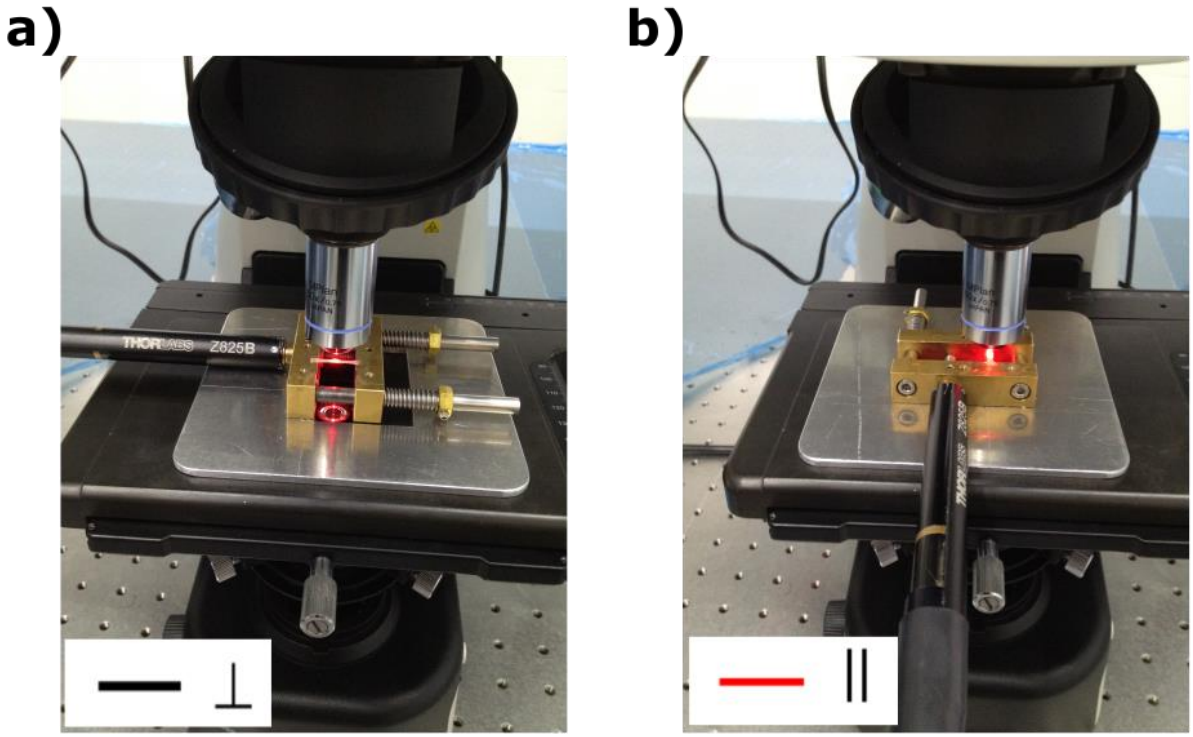

Figure S11. Photographic images showing our polarized Raman setup during measurement of a stretched nanocomposite sample (between the copper bars) when the angle between the incident Raman light polarization and the stretching direction is (a) perpendicular or (b) parallel.